Green icebergs and remote sensing

Raymond L. Lee, Jr.

Department of Meteorology, Pennsylvania State University, University Park, Pennsylvania 16802

Received October 12, 1989; accepted June 7, 1990

The curious phenomenon of green icebergs has fascinated polar travelers for centuries. Although translucent green icebergs might be caused by colorants, a recently obtained sample of a green iceberg contained little inherently green material. This fact, combined with the blue-green absorption minimum of pure, homogeneous ice, suggests that a sufficient (rather than necessary) condition for green icebergs may be reddened sunlight illuminating intrinsically blue-green ice. Lacking *in situ* spectral reflectances of green icebergs, we develop two remote-sensing techniques to analyze their optical properties. Estimates of a green iceberg's reflectance spectra are derived from spectrodensitometry and from video digitizing of original color slides. Proxies for polar daylight spectra yield the iceberg's chromaticities, which agree closely with those predicted by two multiple-scattering theories.

INTRODUCTION

Icebergs are hardly colorless monoliths, and even nominally white bergs routinely display many hues.[1–3] Nonetheless, vivid bottle-green icebergs are remarkable enough to have prompted several short papers.[4–8] (Plates I and II illustrate one such berg.) Obviously the colors of some sea and glacier ice are caused by intrinsically colored[9] minerals or organisms.[10–12] However, ice recently taken from (or near) two green icebergs indicates that these bergs need not be predominated by green inclusions. Amos retrieved an unusual ice sample near a Weddell Sea iceberg that had a dark green outcropping.[7] He noted that the ice sample "was covered with regular hexagonal-shaped depressions . . . [and] appeared colorless in daylight as well as under artificial lighting conditions."[7] When Amos and his colleagues examined thin sections of this putative green iceberg sample, they found "a remarkably bubble-free, highly orientated [sic] crystalline structure" and "a diversified assemblage of particles including a large number of fibers . . . ranging from colorless to blue, orange, and green; obsidian flakes; a few quartz grains; amorphous aggregates; black, charcoal-like fragments; pieces of shelly material; and diatoms . . . ."[7]

Dieckmann *et al.* sampled a Weddell Sea green iceberg directly, and their specimen contained "grey mineral and biogenic material apparently of marine origin" distributed in "relatively well defined layers" throughout.[8] They conclude that "[o]ur analyses and observations confirm that the green colouration was not caused by green pigmentation, but probably by reflection and/or absorption of light due to the more or less densely spaced, parallel layers of incorporated debris. Green feldspars which could have been responsible for the colour were rarely found."[8] They also note that their ice sample "changed from green to a translucent white upon separation from the iceberg."[8] Swithinbank says of this color difference: "Samples [of green or black icebergs] held in the hand have been reported to consist of clear bubble-free ice, providing a conspicuous contrast with the white bubbly ice of which most Antarctic bergs are made."[5] Naturally, definitively answering why some icebergs are green requires further analysis of their composition and structure.[13] However, we pose a narrower question here. Based on the available evidence, might *some* green icebergs be the result of reddened sunlight illuminating blue-green ice?

As Swithinbank notes, only the bubbliness of most glacier and iceberg ice makes it white. Pure, homogeneous ice[14] has an absorption minimum at 470 nm (Fig. 1).[15] If we transmit light that is initially white (i.e., spectrally uniform) through 1 m of this ice, the resulting dominant wavelength would be ~490 nm, a cyan.[16] Thus we say that pure, homogeneous ice is intrinsically blue-green. However, the ice's color will change if we add scatterers or dissolved impurities to it, change its thickness, or view it under chromatic illumination. To date, the spectral properties of green iceberg inclusions remain moot. Since assigning the inclusions a particular color (say, green) lets us make icebergs of any hue, I conservatively assume that the ensemble of scatterers is essentially gray. This is not inconsistent with the observations of Amos and of Dieckmann *et al.* In addition, I assume that if the ice were homogeneous, it would have pure ice's absorption spectrum.

Now we rephrase our question as "How close is the *perceptual* agreement between the observed colors of green icebergs and those predicted by a theory for bubbly (or dirty) ice?" To answer this, I need to extract accurate colorimetric information from my best available sources, three original color slides of Dieckmann's green iceberg. I also require accurate estimates of the daylight spectra that illuminated this berg and a theory that incorporates the salient features of naturally occurring ice.

TWO MULTIPLE-SCATTERING MODELS FOR NATURAL ICE

How can we model the optics of ice associated with green icebergs (i.e., ice containing few bubbles or other scatterers)? Several models describe single and multiple scattering by naturally occurring ice.[17–20] I chose a pair of closely related two-stream multiple-scattering models by Bohren[21,22] and by Mullen and Warren.[23] I selected these models because they are straightforward, relatively complete in their parameterization of natural ice, and seem adequate to describe green icebergs' reflectance spectra. Mul-

0740-3232/90/101862-13$02.00 © 1990 Optical Society of America

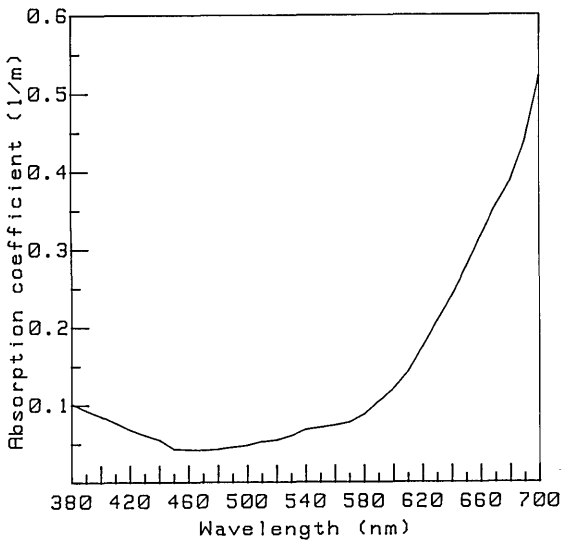

Fig. 1. Absorption coefficient (1/m) for pure, homogeneous ice in the visible; the absorption minimum is at 470 nm. These data are taken from Ref. 15.

len and Warren's parameterization is more elaborate than Bohren's, but both models predict essentially the same ice reflectance spectra in the visible.

We want to describe spectral reflectance that results from multiple scattering by (possibly) absorbing inclusions within a translucent, absorbing medium. We assume that the ice inclusions are spherical, of a single size, and uniformly distributed throughout the ice. Of course, these assumptions are not strictly true in naturally occurring ice, but they are acceptable as parameterizing conditions within already approximate models. Finally, since air bubbles and sediment in icebergs are much larger than the wavelengths of visible light,[8] we can use some approximations that are valid in the limit of large particles.

When combined, the preceding assumptions lead to an expression for the single-scattering albedo $\tilde{\omega}_{0,p}$ of inclusions in dirty or bubbly ice:

$$\tilde{\omega}_{0,p} = \sigma_p/2\pi N_p r_p^{\,2} = \sigma_p/(\sigma_p + \kappa_p), \tag{1}$$

where σ_p is the particles' or bubbles' scattering coefficient, κ_p their absorption coefficient, N_p their number density, and r_p their radius.[24] The subscript p distinguishes the properties of ice inclusions from those of pure, homogeneous ice (subscript i). The absorption coefficient of pure ice (κ_i) depends on wavelength, and so will σ_p in general. However, we start by assuming that we know only how $\kappa_i(\lambda)$ varies (Fig. 1) and that the particles' extinction cross section $C_{\text{ext},p}$ is independent of wavelength. In addition, we assume that ice's molecular scattering is negligible ($\sigma_i = 0$) compared with its absorption. For these reasons, plus the fact that Dieckmann *et al.* call their green iceberg's inclusions gray, we take $\tilde{\omega}_{0,p}$ to be constant in the visible. This is the simplest assumption possible, and it can be modified if need be.

In natural ice, the presence of inclusions effectively changes κ_i. We define the volume fraction f of these inclusions as

$$f = N_p V_p, \tag{2}$$

with V_p being the volume of a single inclusion. The quantity $1 - f$ is the proportion of pure ice in the iceberg, and we can use it to weight κ_i, thereby finding an absorption coefficient for natural ice. Based on definitions of glacier ice,[25] a realistic upper bound on f is 0.1. We can show that the effective single-scattering albedo $\tilde{\omega}_{0,\text{ICE}}$ for the composite medium of natural ice (subscript ICE) is

$$\tilde{\omega}_{0,\text{ICE}} = \sigma_p/[\sigma_p + \kappa_p + (1 - f)\kappa_i]. \tag{3}$$

Using Eqs. (1) and (2), we rewrite Eq. (3) so that

$$\tilde{\omega}_{0,\text{ICE}} = \frac{\tilde{\omega}_{0,p}}{1 + [(1 - f)\kappa_i V_p/fC_{\text{ext},p}]}. \tag{4}$$

Finally, since $V_p/C_{\text{ext},p} = 2r_p/3$ for large spherical particles, we can restate Eq. (4), using variables whose physical interpretation may be somewhat more obvious:

$$\tilde{\omega}_{0,\text{ICE}} = \frac{\tilde{\omega}_{0,p}}{1 + [2(1 - f)\kappa_i r_p/3f]}. \tag{5}$$

The limiting behavior of Eq. (5) makes physical sense. If the particles absorb perfectly, then $\tilde{\omega}_{0,\text{ICE}} = 0$; i.e., photons are absorbed either by the inclusions or by the pure ice, and no radiation entering the iceberg can escape. If $\tilde{\omega}_{0,p} = 1$ (completely nonabsorbing inclusions such as air bubbles), then $\tilde{\omega}_{0,\text{ICE}} \approx 1$; losses are due only to absorption by the ice. For example, for air bubbles, an intermediate value of $\kappa_i(\lambda)$, a volume fraction of 0.05, and an inclusion radius of 0.1 mm, we have $\tilde{\omega}_{0,\text{ICE}} = 0.9997$. In fact, for a wide range of realistic r_p, $\tilde{\omega}_{0,p}$, and f, $\tilde{\omega}_{0,\text{ICE}}$ will be only slightly less than 1.

The theory of Mullen and Warren does not require detailed knowledge of the inclusions' scattering phase function, and thus the asymmetry parameter g adequately summarizes angular scattering by particles. Strictly speaking, g is a function of wavelength, but Mullen and Warren show that, for air bubbles, g varies insignificantly in the visible. When comparing measurements of green ice spectra with those from models, I also assume that the unknown $\tilde{\omega}_{0,p}$ and g are independent of wavelength. Even if g varies spectrally for inclusions other than air bubbles, only the details, rather than the substance, of my conclusions should be affected. In other words, the magnitudes of $\tilde{\omega}_{0,p}$ and g required to make a given iceberg would change, but the fact that internal scatterers of some kind can cause green icebergs should not.

Choosing constant $\tilde{\omega}_{0,p}$ and g also means that we have effectively precluded Mie theory's fine spectral detail. Mullen and Warren consider whether Mie theory is appropriate for an absorbing medium such as ice and ultimately decide to use approximations. For us the choice is simpler; the colorimetric effects of the Mie ripple structure are likely nil. In addition, our models' assumption of average r_p and N_p is equivalent to integrating over a particle-size distribution in natural ice. This in itself would obscure small-scale spectral detail such as the ripple structure.

Mullen and Warren not only account for scattering within an ice slab but also consider internal and external specular reflection at the ice–air boundary. Based on the work of Wiscombe and Warren[26] and that of Joseph *et al.*,[27] they develop a model for ice albedo that they call the "specular delta–Eddington" method. The specular delta–Eddington albedo (here denoted a_{SDE}) is a hemispheric albedo[28] for specularly reflecting ice and is given by

$$a_{\mathrm{SDE}} = R_1 + \frac{(1 - R_1)A(\theta_1)(1 - R_2)}{1 - R_2 A_d}. \tag{6}$$

a_{SDE} is the sum of an infinite series, the first term of which is the external specular reflectance R_1.[29] The second term in Eq. (6) describes what happens when a sunbeam forms an incidence angle θ_0 with an ice surface that is locally planar. The sunbeam is refracted at an angle θ_1 to the ice surface's normal. The delta–Eddington approximation alone (i.e., without internal or external specular components) predicts that this direct beam within the ice results in a multiple-scattering contribution of $A(\theta_1)$ to a_{SDE}. A_d in Eq. (6) arises from radiation that has been multiply scattered by inclusions and repeatedly reflected at the ice–air boundary before leaving the ice. Although this internal radiation field is relatively isotropic, its source, internal specular reflections from the ice–air interface, need not be.[26] The factor of R_2 is an average Fresnel reflection coefficient for all internal angles of incidence at the ice–air boundary.

After describing the same single-scattering quantities (i.e., $\tilde{\omega}_{0,p}$ and g) as Mullen and Warren, Bohren develops an equation for $1 - \tilde{\omega}_{0,\mathrm{ICE}}$ that is valid in the geometric-optics limit.[21] This can be rewritten as

$$\tilde{\omega}_{0,\mathrm{ICE}} = 1/[1 + 2(1 - f)\kappa_i r_p/3f], \tag{7}$$

with all variables defined as above. As it stands, Eq. (7) is valid only for bubbles and other nonabsorbing scatterers. To overcome this minor limitation, Eq. (7) can be replaced by Eq. (5) (the two equations differ by a factor of $\tilde{\omega}_{0,p}$). As Mullen and Warren note, Bohren's formula for the hemispheric albedo of bubbly ice[21] can be rewritten to be accurate over a wider spectral range. Both of these changes are made by substituting Eq. (5) into Bohren's expression for the hemispheric albedo of an optically thick absorbing medium.[22] This yields

$$a_{\mathrm{CB}} = \frac{(1 - \tilde{\omega}_{0,\mathrm{ICE}} g)^{1/2} - (1 - \tilde{\omega}_{0,\mathrm{ICE}})^{1/2}}{(1 - \tilde{\omega}_{0,\mathrm{ICE}} g)^{1/2} + (1 - \tilde{\omega}_{0,\mathrm{ICE}})^{1/2}}, \tag{8}$$

in which the subscript CB indicates the ice albedo associated with Bohren's model. Bohren is not concerned with specular reflection by the ice, and he also assumes isotropic illumination. These differences mean that a_{CB} will usually generate larger albedos than either a_{SDE} or its nonspecular counterpart $A(\theta_1)$. However, Bohren's model produces reflectances that are quite accurate spectrally.[30] If we are less interested in albedo than in spectral reflectances (as will often be true in colorimetry), then the simpler calculations of a_{CB} will be advantageous.

ESTIMATING POLAR DAYLIGHT SPECTRA

Reconstructing the colors of the green iceberg in Plates I and II would be easier if we had detailed spectra of the daylight illuminating the berg. That we do not is a natural corollary of our particular remote-sensing technique; if we had *in situ* daylight spectra, we also would have detailed iceberg spectra. In fact, the *raison d'être* of measuring iceberg colors remotely is to see what kind and quality of information can be extracted from readily available sources of information such as photographs.

Thus for now we will work with estimated daylight spectra. These estimates may derive from theory, observations, or some blending of the two. However, aside from the study by Grenfell and Perovich of solar irradiance off the northern coast of Alaska,[31] most published irradiance spectra have been measured outside the polar regions.[32] With one exception, the spectra cited above are presented either graphically or in statistically reduced form. The problems of adapting these spectra to colorimetry seem more onerous than making our own measurements. More important, these earlier daylight measurements usually are inappropriate for our needs. As Condit and Grum noted some years ago, researchers are interested in zenith daylight, north sky daylight, or direct sunlight but seldom in daylight spectra illuminating nearly vertical surfaces that are seen under a wide variety of solar elevations and azimuths.[33] Published data on this last-named kind of daylight spectra are still quite scarce.

Although many empirical relationships between scattering models and daylight spectra have been proposed over the years,[34–36] the sheer number of these hybrids discourages their use. Namely, how do we select the modified theory most appropriate to polar daylight? The answer is that there is no good way of choosing unless we already have polar spectra, and, as we have seen, these are in short supply. Using a more rigorous scattering approach, such as applying Mie theory to polydispersions typical of the polar marine atmosphere, might seem desirable. However, there are two problems with this approach. One is that we have not avoided empirical approximations, since a particle-size distribution must be specified for this polar atmosphere and such curves typically take the form of a power-law fit to observed aerosol size distributions. Models of haze droplet-size distributions illustrate the point, and McCartney describes several of the choices available.[37] Shaw has published some high-latitude measurements of spectral optical thicknesses that are due to atmospheric aerosols.[38] These data could be adapted for use in a scattering model, although we would once again be adding uncertainty to the calculations: errors in the original data could be compounded by extrapolating to unknown conditions on the Weddell Sea. A second problem with the rigorous approach is that, colorimetrically speaking, it is overkill. First, integration over a particle-size distribution would smooth the small-scale spectral features of the monodisperse Mie calculations, features that were resolved only at great computational expense. Second, colorimetric variables are even more unlikely to benefit from these computational heroics, since a relatively large spectral integration step is standard practice in colorimetry.

Given these uncertainties, extrapolation from locally measured daylight spectra to unknown polar ones seems an entirely adequate way of estimating iceberg illumination. Naturally, this extrapolation requires some care. When measuring hemispheric spectral irradiances of daylight, I matched local sky conditions as closely as possible to those in Plates I and II; that is, irradiance measurements were made under clear skies. Since colorimetry is usually concerned with the spectral distribution (rather than the magnitude) of irradiances, not having a day with cloud cover identical to that in Dieckmann's photographs is unlikely to be a critical problem. This is not to dismiss the issue, since daylight spectra do shift as sky conditions range from clear to overcast.[31,33] However, given the small difference in cloud cover between the time of the Weddell Sea photographs and that

of our measurements, any spectral mismatch between the two cases is likelier to arise for other reasons.

Daylight spectra may differ simply because inland Pennsylvania is not an Antarctic sea. Optically, the two locations differ both above and below the horizon. As Grenfell and Perovich note, "the lower troposphere over summer sea ice is, as a rule, saturated with water vapor, even on clear days . . . ."[31] This need not be true in central Pennsylvania. However, for a given solar elevation at either location, variations in water-vapor content (and thus haze concentration) are likely to have the largest effect on daylight spectra. In other words, although concentrations of other aerosols are likely to differ at the two locations, the most important spectral changes in daylight are likely to arise from daily variations in haze droplet concentrations.[38] Although spectral scattering cannot be compared quantitatively at the two locations, I assume that if visibility differences are imperceptible, then so are differences in daylight color that arise from atmospheric scattering.

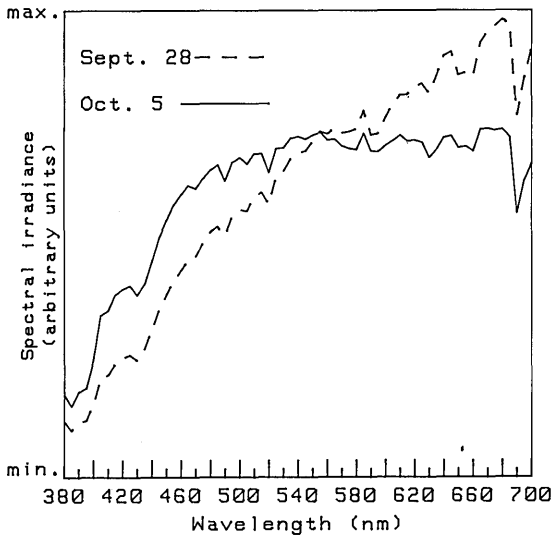

Fig. 2. Daylight spectral irradiances for 18° solar elevation and 0° relative azimuth on September 28 (dashed curve), and October 5 (solid curve), 1987, at University Park, Pennsylvania. The curves are normalized by their respective sums to emphasize spectral differences in atmospheric scattering. The sum of the October 5 irradiances is 3.28 times that of September 28.

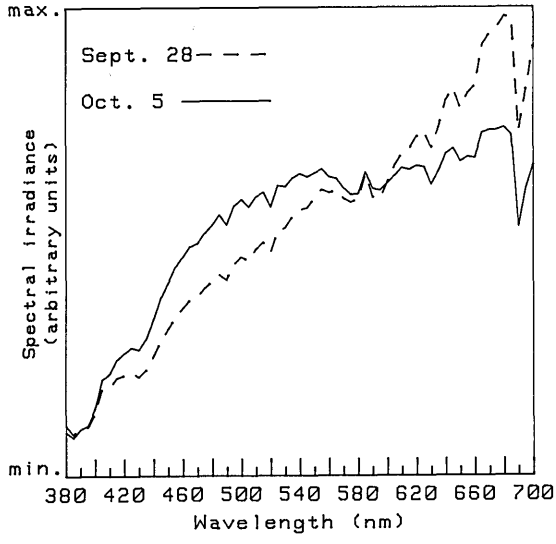

Fig. 3. Normalized daylight spectral irradiances for 10° solar elevation and 0° relative azimuth on September 28 (dashed curve), and October 5 (solid curve), 1987, at University Park, Pennsylvania. The sum of the October 5 irradiances is 6.0 times that of September 28.

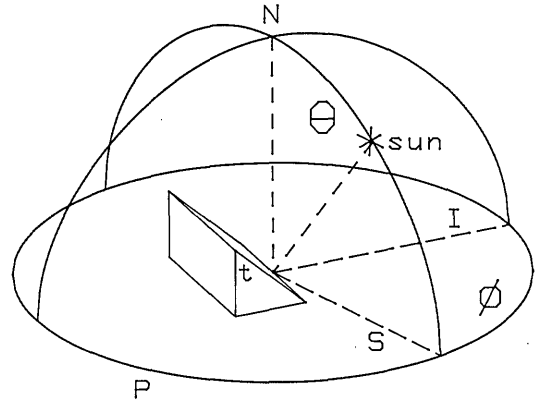

Fig. 4. Geometry of the instrument setup used to measure daylight irradiances. The spectroradiometer is represented by the prism that sits on the tangent plane P. A normal to this plane, N, points toward the zenith. A line drawn from the instrument toward the sun forms the zenith angle θ with N. The front surface of the spectroradiometer's detector is tipped at an angle t from the zenith (t = 15° here). A normal projected from the detector onto the tangent plane results in the line I, the instrument azimuth. The solar azimuth (line S) is defined by a similar projection of the angle θ. The angle between I and S is the relative azimuth ϕ.

As a further precaution in my colorimetric calculations, I have used local irradiance data taken on two different afternoons. Although skies were clear on both days (September 28 and October 5, 1987), visibility was distinctly better on the latter date. Spectral irradiances measured for the same solar elevations on the two days show how daylight color shifted (Figs. 2 and 3). In both cases, the spectroradiometer faced the sun in azimuth, and its detector was tipped 15° from the vertical. Figure 4 schematically illustrates how the spectroradiometer was set up. I have discussed elsewhere how the daylight spectra were measured as well as described an interpolation algorithm for applying them to a wide range of solar elevations and azimuths.[39]

To bracket my colorimetric measurement of Dieckmann's green iceberg, I made separate calculations in which I assumed that the spectral irradiance on the Weddell Sea was represented by the spectra from either September 28 or October 5. As a practical matter, any uncertainty about the time of day (i.e., solar elevation) at which Plates I and II were taken is comparable to the uncertainty about haze concentrations in the scene. This means that if we estimate the green iceberg's color over a range of solar elevations or use the two local atmospheric scattering cases, we will have likely spanned the range of our errors in estimating atmospheric spectral scattering on the Weddell Sea. Differences in surface albedos do exist at the two locations. However, since my spectroradiometer's field of view was blocked below the astronomical horizon and was unobstructed above it, the resulting daylight spectra should be little influenced by

the surroundings. Similarly, photometric measurements of Plates I and II indicate that the sea is dark enough that it contributes negligibly to the iceberg's illumination.

PSYCHOPHYSICS, COLORIMETRY, AND GREEN ICEBERGS

Thus far I have concentrated on explaining green icebergs physically. Ultimately, we want to know whether our physical models account for the icebergs' appearance. Part of our answer comes from comparing calculated chromaticities of green icebergs with those reconstructed from Plates I and II. However, colorimetry alone cannot account for all the perceptual issues associated with green icebergs. Among these are simultaneous color contrast, memory color, and color constancy.

We do not know whether color contrast or other opponent color phenomena affect iceberg colors. Nevertheless, we should not sanguinely dismiss the possibility that, say, yellow induced within an iceberg's outline by a blue surround (sea and sky) enhances its greenness. Color constancy and memory color are not completely independent, since the former depends not only on how quickly the ambient illumination changes but also on whether we assume that we know an object's inherent color. Although the notion of inherent color is physically specious, daily experience reinforces the idea that particular objects have particular colors. Perceptual resistance to changes in an object's memory color can be quite entrenched.[40] Of course, we are claiming that color constancy and memory color begin to fail when we see *some* icebergs in reddened daylight and that the bergs become appreciably greener.

The effects of color constancy, memory color, and color contrast on our perception of green icebergs have yet to be quantified. Thus for now I will use colorimetric analysis of photographs as a useful, if incomplete, way of quantifying those perceptions. One convenient way of extracting colorimetric data from photographs is to digitize the photographs with a color television camera and electronic digitizing system. However, before we can make any colorimetric sense of these data, we need to describe how the various trichromatic systems involved (color film, red–green–blue television cameras, and our visual system) render a wide range of spectra. In general, the spectral transfer functions of these systems are not linearly related. Horn has demonstrated that, if the systems are not related linearly, then stimuli that are metameric for one such trichromatic system need not be metameric for the others.[41] In the case of a video digitizing system, these differences in metamerism will not be critical unless they are so pervasive that the system is a poor proxy for human color vision. Assuming that the differences are not pervasive, the chief problem is to calibrate the video digitizing system both colorimetrically and photometrically. I have earlier described an algorithm for doing this.[42]

Although video digitizing systems are versatile, they do have limitations. For example, digitizers typically have smaller radiance dynamic ranges than do radiometers. If the transmittance of a black area on a color slide is 0.2% and that of a white area is 70%, the resulting 350-fold increase in transmitted radiance can overwhelm either a video camera's pickup tubes or a digitizer's analog-to-digital converter. In other words, a slide whose transmittance dynamic range is this large (or even smaller) can drive either video device to its maximum output. Many radiometers can easily accommodate this range of transmitted radiances. Radiometers also offer superior radiance resolution for extremely small or large film densities. With these advantages in mind, I have also developed an algorithm for colorimetric calibration of a spectrodensitometer that analyzes color slides.[39] Tests of this technique indicate that its colorimetric accuracy is comparable to that of video digitizing. Both systems reconstruct metameric spectral reflectances that are colorimetrically accurate, which is our overriding concern in analyzing green iceberg photographs.

Using either system requires some caution. Both rely on photographing a color calibration card under the same daylight illumination as that in a scene of interest. Some potential error arises from differences in color film, for which spectral response can shift subtly with each new lot manufactured. More important, different exposure and processing conditions can introduce color discrepancies within identical film stock. This does not mean that attempting to extract colorimetric information from slides is hopeless. Such techniques can closely identify color samples that are photographed under the same illumination as the color calibration card.[39,42] However, like other remote-sensing techniques, spectrodensitometry and video digitizing necessarily involve uncertainties that would not exist if we could measure unknown color samples directly. On balance, then, properly calibrated video and spectrodensitometry systems will reconstruct similar, but not identical, chromaticities and relative luminances.

RECONSTRUCTING THE COLORS OF GREEN ICEBERGS

When using video digitizing, we can easily show which locations on Plates I and II have been sampled, and do so in Figs. 5 and 6. (In addition to colorimetric analysis of Plates I and II, I will also show results from a third original slide of this iceberg, also taken at the same time and location by Dieckmann.) Two sampling methods are used in digitizing. In one, the red, green, and blue (RGB) pixel values at an image location are averaged over an area 10 pixels square; these average RGB values are then passed to the inversion scheme described in Ref. 42. These sampling areas are indicated by ×'s in Figs. 5 and 6. The second sampling technique measures RGB values along a line in the digitized image. Figures 5 and 6 show two such sampling lines as the line segments *CD* and *EF*. Note that these largely avoid regions on the iceberg that are either in shadow or dominated by specular reflections.

Now we can estimate the chromaticities of the iceberg in Plates I and II. Figure 7 shows a portion of the 1931 CIE chromaticity diagram. In it, the chromaticity of the sun outside the atmosphere ($x = 0.3171$, $y = 0.3263$) has been marked with an $*$. This reference point is repeated in Figs. 8–12. Another colorimetric reference introduced in Fig. 7 is a rhomboidal locus of chromaticities generated by the SDE model. This box of chromaticities is constructed as follows.

First, assume that we can describe our uncertainty about spectral irradiance by using the range of solar elevation angles occurring during Dieckmann's observation of the iceberg. Astronomical calculations set this elevation range at

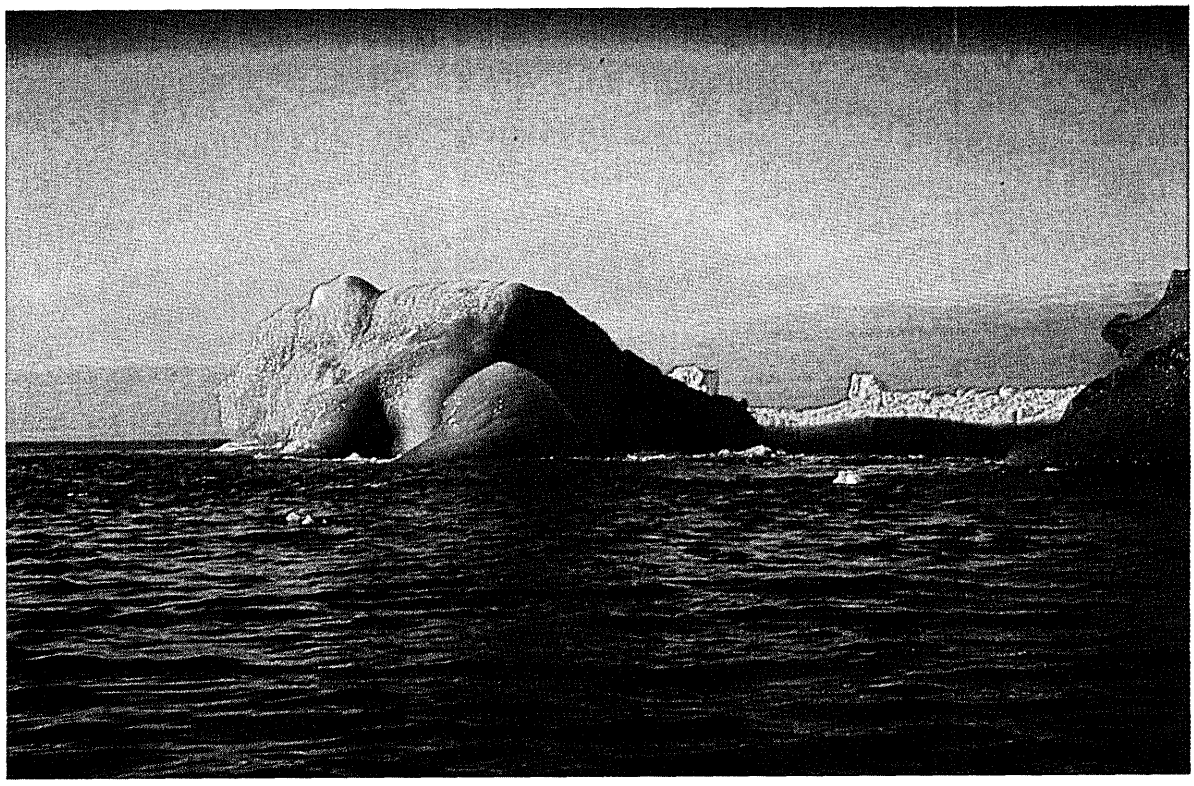

Plate I. Green iceberg sighted off Kapp Norvegia, Weddell Sea, Antarctica, on February 16, 1985, between 1700 and 2000 GMT. Photograph courtesy of G. Dieckmann.

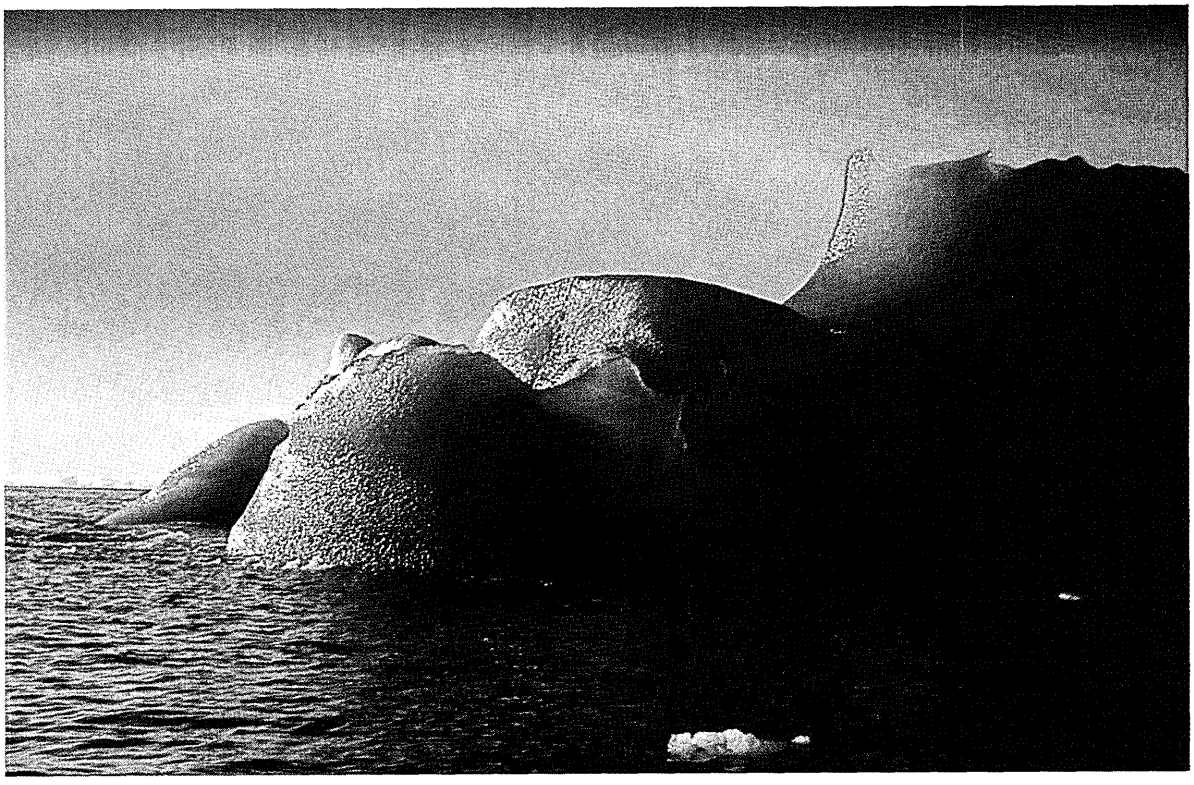

Plate II. Green iceberg sighted off Kapp Norvegia, Weddell Sea, Antarctica, on February 16, 1985, between 1700 and 2000 GMT. Photograph courtesy of G. Dieckmann.

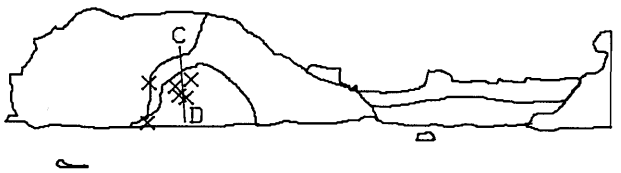

Fig. 5. Sketch of the principal features of Plate I. The ×'s mark the sites of digitized RGB samples and span an area slightly larger than that sampled. Chromaticities for these samples are shown in Fig. 11 below. The line *CD* is the location of RGB samples whose chromaticity curve is shown in Fig. 8.

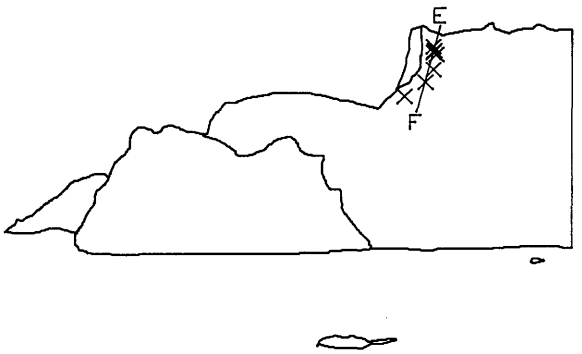

Fig. 6. Sketch of the principal features of Plate II. The ×'s mark the sites of digitized RGB samples and span an area somewhat larger than that sampled. Chromaticities for these samples are shown in Fig. 12 below. The line *EF* is the location of RGB samples whose chromaticity curve is shown in Fig. 9.

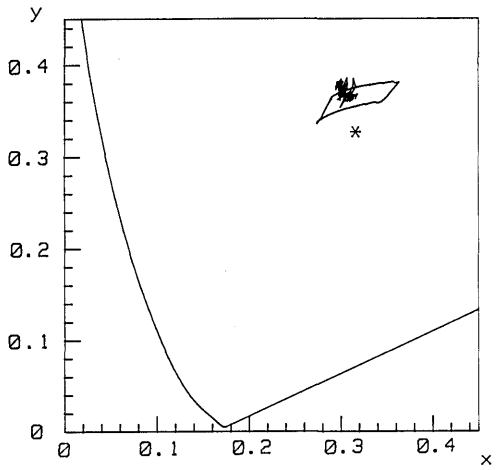

Fig. 7. Portion of the 1931 CIE chromaticity diagram. The * is the chromaticity of the sun outside the atmosphere, and the rhomboidal box is the locus of green iceberg chromaticities generated by the SDE model for the estimated range of spectral illumination in Plates I and II. The chromaticity curve is generated by a linear scan in one of Dieckmann's green iceberg photographs.

approximately 22° to 9°, which gives us a gamut of possible illuminants in Plates I and II. Second, rather than varying both the scatterers' optical properties (variables g and $\tilde{\omega}_{0,p}$) and their distribution (variables r_p and N_p) in a_{SDE}, we use only air bubbles ($\tilde{\omega}_{0,p} = 1$, $g = 0.845$) (Ref. 21) to draw Fig. 7's chromaticity box. There we vary r_p and N_p over a realistic range (the inclusion volume fraction f never exceeds 0.1). Our choice of possible reflectance spectra (and thus of chromaticities) is conservative; as Dieckmann *et al.* indicate, inclusions other than air bubbles are found in green icebergs.[8]

The chromaticity box's top line consists of colors generated by all ice reflectance spectra at 9° solar elevation. The bottom of the box shows the corresponding chromaticities at 22° solar elevation. As expected, purer ice colors are associated with purer daylight colors. The left-hand side of the box is the chromaticities that result when all daylight spectra illuminate the most spectrally selective ice. Conversely, the box's right-hand side is produced by the full gamut of daylight illuminating the spectrally flattest ice. Within the chromaticity box are the possible colors for ice whose only inclusions are bubbles, so our reconstructed chromaticities need not fall entirely within it.

Photogrammetry suggests a solar elevation of 18° in Plates I and II. Figure 2 compares the September 28 and October 5 daylight spectra for this solar elevation. Of these two spectra, I chose the October 5 case (solid curve) because visibility on that day was qualitatively closer to that in Plates I and II. None of this approximation is critical, since we are merely selecting one spectrum from a range of

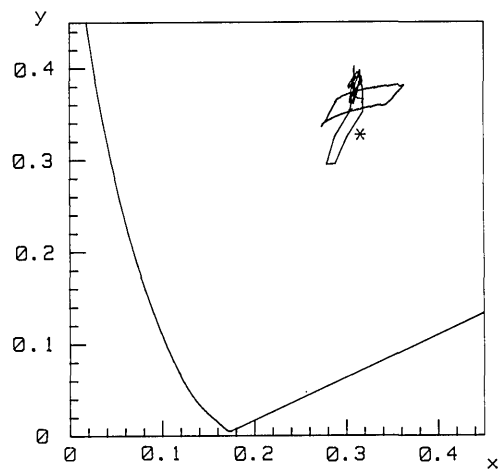

Fig. 8. A portion of the 1931 CIE chromaticity diagram. The chromaticity curve is generated by scanning Plate I along the line *CD* in Fig. 5.

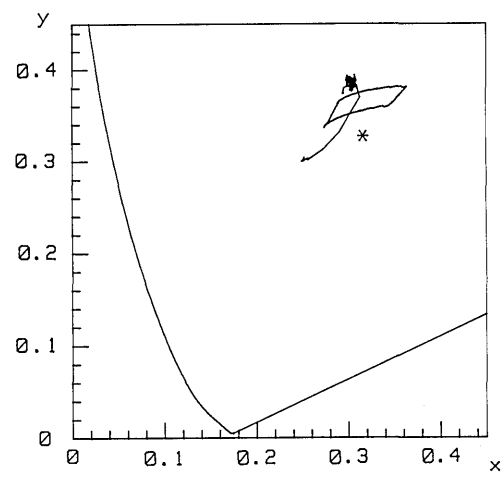

Fig. 9. Portion of the 1931 CIE chromaticity diagram. The chromaticity curve is generated by scanning Plate II along the line *EF* in Fig. 6.

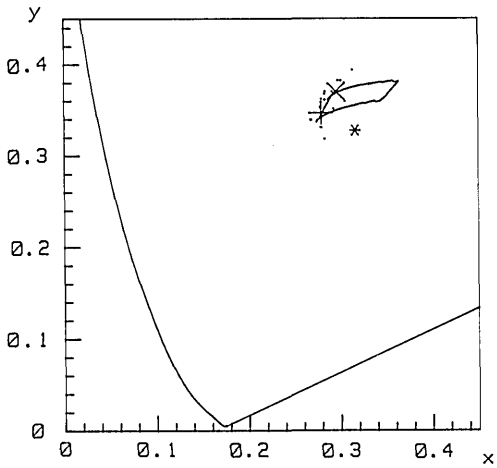

Fig. 10. Green iceberg chromaticities generated by spectrodensitometry and video digitizing (small dots) for one of Dieckmann's green iceberg photographs. The average chromaticity from densitometry is drawn as a + (albedo 13.6%, $x = 0.2795$, $y = 0.3462$). The average chromaticity from digitizing is drawn as an × (albedo 17.0%, $x = 0.2957$, $y = 0.3699$).

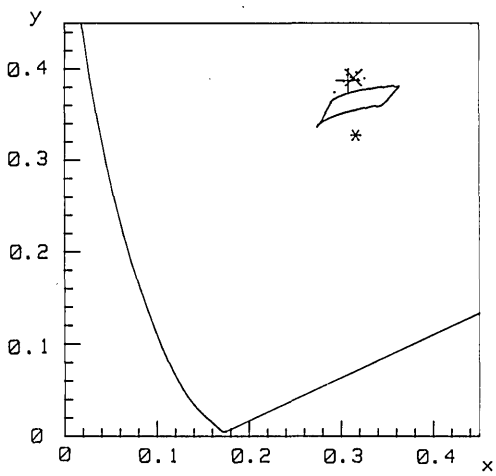

Fig. 11. Green iceberg chromaticities generated by spectrodensitometry and video digitizing (small dots) for Plate I. The average chromaticity from densitometry is drawn as a + (albedo 26.0%, $x = 0.3083$, $y = 0.3871$). The average from digitizing is drawn as an × (albedo 16.7%, $x = 0.3141$, $y = 0.3901$).

possibilities, and ultimately we are interested in how well our theoretical and reconstructed chromaticities agree within this range. As a result, although the 18° spectrum is used in calculating chromaticities from our reconstructed reflectance spectra, our conclusions are not crucially linked to this particular illuminant.

Figure 7 implies that spectrally selective ice will have *some* color even when the sun is high in the sky. In other words, icebergs that are vividly green near sunset may still be greenish or bluish green at noon (neglecting color constancy). The effect of a low sun is simply to increase the dominant wavelength and change the purity of these bergs. For example, at 9° solar elevation the most spectrally selective ice yields a dominant wavelength of 509 nm and a purity of 9%, measured with respect to the * in Fig. 7. We would probably call this ice green. However, when the solar elevation is changed to ~41° (the yearly maximum at the location of Plates I and II), the same ice seen under this new illumination has a dominant wavelength of 488 nm and a purity of 23%. We would now likely say that the ice was bluish-green (again neglecting color constancy).

Figure 7 shows a chromaticity curve that results from scanning along a line in the third of Dieckmann's green iceberg photographs (not reproduced here). This kind of zigzag chromaticity path is typical of many seemingly uniform colors, including the individual chips on the color calibration card. Of special interest to us is the relatively small area that the path occupies, a square approximately 0.03 on a side on the chromaticity diagram. Thus the digitizing algorithm produces a restricted set of chromaticities for a restricted range of RGB values. Even though this particular green iceberg's inclusions are probably not dominated by air bubbles, the observed chromaticities are nonetheless largely inside the chromaticity box for bubbly ice.

Figure 8 shows the green iceberg chromaticity curve generated along the scan line *CD* in Fig. 5. As in Fig. 7, the chromaticity gamut is small, with the exception of one large excursion toward the violet, which occurs when we cross into shadow in Plate I. Since the illumination changes dramatically (it is primarily skylight in this region of the berg), the chromaticity will change equally dramatically. Certainly the reconstructed spectra are implausible in the shadows, making the resulting chromaticities and albedos only qualitatively correct.

The locus of chromaticities in Fig. 9 is generated along scan line *EF* in Fig. 6. On average, purities are higher here than in the preceding cases. Before making too much of this, remember that the spectral illumination varies enough between Plates I and II to account for some of the difference. No less likely is the existence of real differences in spectral reflectance (or transmittance) due to variations in ice composition and optical depth. The most striking feature of Fig. 9 is the large excursion into the blue. Unlike that in Fig. 8, we can believe this large chromaticity change: it occurs as we briefly traverse some blue sky (point E in Fig. 6).

We now switch to areal averages of green iceberg colors.

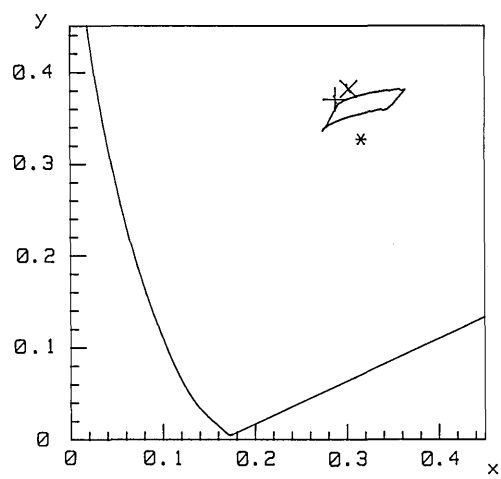

Fig. 12. Green iceberg chromaticities generated by spectrodensitometry and video digitizing (small dots) for Plate II. The average chromaticity from densitometry is drawn as a + (albedo 18.0%, $x = 0.2878$, $y = 0.3703$). The average from digitizing is drawn as an × (albedo 14.4%, $x = 0.3025$, $y = 0.3818$).

In Figs. 10–12 we compare spectrodensitometry's results with those from video digitizing. The small dots are chromaticities reconstructed by both techniques at various image locations. Although we cannot specify the photographic sites of the densitometry samples exactly, examining the same readily identifiable features with either technique gives comparable colorimetric averages. The average of all chromaticities reconstructed by densitometry is indicated with a + in Fig. 10; the corresponding video average is indicated with an ×. We continue this marking scheme in Figs. 11 and 12.

The colorimetric disagreement between densitometry and video digitizing is largest in Fig. 10; the colorimetric distance between the two averages is 0.0287, although the biconical albedos differ by only 3.4%. Given the closer agreement in Figs. 11 and 12, and the difficulty of specifying image locations when using the radiometer, this colorimetric disagreement seems acceptable. Densitometry indicates that the ice has a dominant wavelength of 498 nm and a purity of 12.4%, while digitizing gives figures of 519 nm and 8.6%. (All dominant wavelength and purity measurements are with respect to the sun outside the atmosphere.) Given the large number of sampling sites here, we will use the spectrodensitometry averages of chromaticity and spectral reflectance when we compare theory and observation below.

Figure 11 shows the best colorimetric agreement between the two techniques; the distance between the averages is 0.0065. However, there is now a more substantial 9.3% disagreement about the ice's albedo. From densitometry, the dominant wavelength of the average chromaticity is 544 nm, and its purity is 15.1%; comparable figures from digitizing are 550 nm and 17.4%. Finally, Fig. 12 offers perhaps the best agreement between densitometry and video analysis. The colorimetric distance is 0.019, and the albedo difference 3.6%. The chromaticities yield a dominant wavelength of 512 nm and a purity of 9.8% for densitometry, while the values are 536 nm and 12.3% for digitizing.

What conclusions can we draw from these results? The most important conclusion is that these numbers are inherently volatile. Moving our sampling sites within the images or changing the size of our areal averages will almost invariably give different results. Complicated natural scenes like those in Plates I and II behave in this way because their spectral radiances (and thus chromaticities) change appreciably within small areas. Therefore the substantial although imperfect colorimetric agreement between the two data inversion techniques implies that their precision is comparable.

A second, more surprising, conclusion is that many natural objects and light sources have rather low colorimetric purities. The highest purity reported above is less than 20%, a number that seems incongruously small compared with the vivid greens in Plates I and II. However, the chromaticity gamut of the color calibration card in Ref. 42 is instructive here. Although the yellowish illuminant (a slide projector) used in these earlier tests shifts the reds and yellows to high purities, most greens and blues will be comparatively unchromatic. Consider another example. Bohren and Fraser note that the blue sky in a purely molecular, single-scattering atmosphere would have a purity of less than 42%.[43] Realistically, the sky's purity will be lower than this, even though we perceive sky color well away from the horizon to be rather vivid. Our own measurements indicate that typical blue sky purities are approximately 25–30% (dominant wavelength ~485 nm). Since we seldom see spectrally pure blues or greens in nature, even the modest purities of the blue sky and this green ice are visually striking. Another important point is that dominant wavelength can change rapidly for small chromaticity changes at low purities. Thus hue seems to shift appreciably when we compare the densitometry and digitizing averages in Figs. 10–12. Perceptually, however, the color changes are likely to be small.

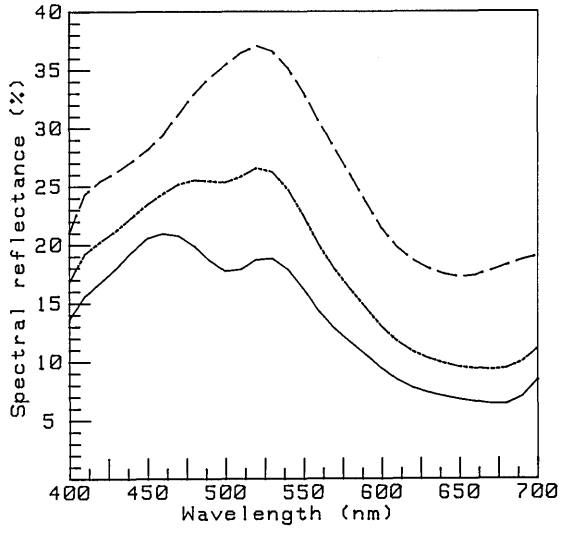

Fig. 13. Average spectral reflectances reconstructed by densitometry for selected locations in Plate I (dashed curve; albedo 26.0%), Plate II (dotted–dashed curve; albedo 18.0%), and another of Dieckmann's green iceberg photographs (solid curve; albedo 13.6%).

Average spectral reflectances reconstructed by densitometry from Dieckmann's color slides appear in Fig. 13. The largest reflectances (dashed curve) are those that generated the + in Fig. 11, and the biconical albedo here is 26%. The dotted–dashed curve corresponds to the + chromaticity in Fig. 12 and has an albedo of 18%. The smallest albedo in Fig. 13 (solid curve) is 13.6%, and its corresponding chromaticity is marked with a + in Fig. 10. As noted above, these are metameric reflectance curves that cannot be expected to do more than reproduce chromaticity and albedo accurately. These curves are unlikely to be identical to *in situ* spectra of Dieckmann's green iceberg. However, because the calibration card's colors are spectrally similar to those of naturally occurring materials,[44] the reconstructed spectra should not differ radically from those of the green iceberg.

HOW MIGHT GREEN ICEBERG THEORY AND OBSERVATION AGREE?

Remember that we are outlining sufficient, rather than necessary, conditions here for green icebergs' inclusions. In addition, note that the Bohren and SDE models describe hemispheric albedos, rather than the biconical albedos reconstructed above, although these differences are likely small in our case. Now, assuming that we know θ_0, N_p, and r_p, what values of $\tilde{\omega}_{0,p}$ and g in the SDE model would minimize colorimetric error and produce acceptable albedo errors compared with our observations?

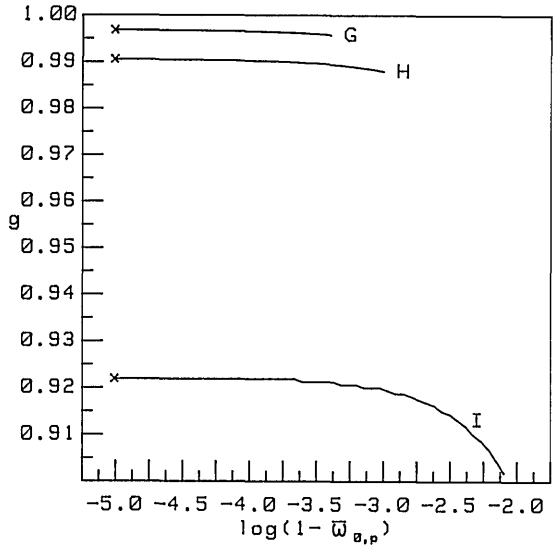

Fig. 14. Loci of $\tilde{\omega}_{0,p}$ and g that yield minimal chromaticity errors (within a ±2% albedo error tolerance) when SDE reflectances are compared with the average spectral reflectances reconstructed by densitometry for one of Dieckmann's green iceberg photographs. Case G sets $r_p = 0.04$ mm and $N_p = 5.26$ mm^{-3}, case H sets $r_p = 0.1196$ mm and $N_p = 0.1966$ mm^{-3}, and case I sets $r_p = 1.0$ mm and $N_p = 3.36 \times 10^{-4}$ mm^{-3}. The X's on curves G–I are the smallest colorimetric errors for each case. In case G, this corresponds to $\tilde{\omega}_{0,p} = 0.9999$, $g = 0.9968$. In case H, the smallest minimum occurs at $\tilde{\omega}_{0,p} = 0.9999$, $g = 0.9905$, and in case I it occurs at $\tilde{\omega}_{0,p} = 0.9999$, $g = 0.9219$.

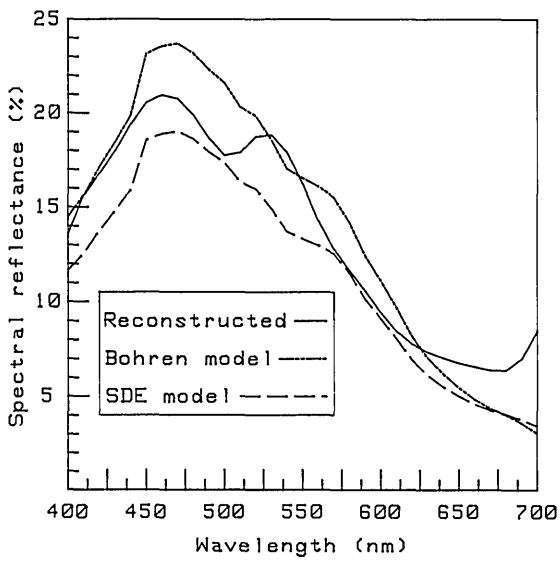

Fig. 15. Spectral reflectances from the SDE model (dashed curve) and the Bohren model (dotted–dashed curve) that are metamers for the average spectral reflectances reconstructed by densitometry from one of Dieckmann's green iceberg photographs (solid curve). The Bohren model assumes an effective grain diameter of 2298 mm. The input parameters to the SDE model are $r_p = 0.1196$ mm, $N_p = 0.1966$ mm^{-3}, $\tilde{\omega}_{0,p} = 0.9999$, and $g = 0.9905$. The root-mean-square reflectance difference between the reconstructed reflectances and the Bohren model is 2.2%. The root-mean-square difference between the SDE model and the reconstructed reflectances is 2.3%.

Figure 14 shows the curves of $\tilde{\omega}_{0,p}$ and g that minimize colorimetric errors for a target chromaticity of $x = 0.2795$, $y = 0.3462$ and an albedo of 13.6% (these are the densitometry averages shown in Fig. 10). The solar elevation is assumed to be 18°, and θ_0 is set at 30°. The curves G–I are the loci of $\tilde{\omega}_{0,p}$ and g that result in the smallest chromaticity errors within an albedo error tolerance of ±2%. Note that the abscissa is $\log_{10}(1 - \tilde{\omega}_{0,p})$. In curve H, the values of r_p and N_p (0.1196 mm and 0.1966 mm^{-3}, respectively) are those estimated from the thin section of a green iceberg. While leaving the volume fraction f unchanged at 0.0014, we increase r_p to 1.0 mm in curve I and decrease it to 0.04 mm in curve G. Although each of these curves generates minimal chromaticity errors, one point on each curve yields the smallest of these minima. We indicate this combination of $\tilde{\omega}_{0,p}$ and g with an X. The chromaticity errors at these points range between 0.0031 and 0.0036 for cases G–I.

In essence, Fig. 14 says that the observed color and albedo of Dieckmann's green iceberg are best matched in the SDE model if the ice inclusions are nearly nonabsorbing ($\tilde{\omega}_{0,p} \approx 1$) and scattering is largely in the forward direction ($0.9 < g < 1$). In fact, because the observed chromaticity falls so close to the box of SDE model chromaticities for air bubbles (see the + in Fig. 10), we might imagine that $\tilde{\omega}_{0,p} = 1$. While completely nonabsorbing inclusions would account for the minimum chromaticity errors occurring at the largest values of $\tilde{\omega}_{0,p}$ in Fig. 14, they are not what Dieckmann *et al.* observed. If we select a different target chromaticity that lies farther outside the chromaticity box, the minimum colorimetric error occurs at smaller $\tilde{\omega}_{0,p}$ (farther to the right in Fig. 14). In physical terms, this change in target chromaticity means that we must allow absorbing inclusions in the ice.

The dashed curve in Fig. 15 is the metameric spectral reflectance curve that generates the minimum colorimetric error in case H of Fig. 14 (the case of $r_p = 0.1196$ mm, $N_p = 0.1966$ mm^{-3}). Figure 15 also includes the reconstructed reflectance spectrum from Fig. 13 that we are trying to match; it is redrawn in Fig. 15 as a solid curve. The minimum-error model spectra for cases G and I in Fig. 14 would be virtually identical. This spectral similarity among the metameric model reflectances may seem odd. However, remember that the spectral variation in these model reflectances arises from one material, pure ice, and its absorption coefficient $[\kappa_i(\lambda)]$. Thus nearly metameric reflectances will have the same spectral shape.

I have also included metameric spectral reflectances from Bohren's model in Fig. 15 (dotted–dashed curve). Because the observed chromaticity can be nearly matched by purely bubbly ice, I have set $\tilde{\omega}_{0,p} = 1$ and $g = 0.845$ in Eqs. (5) and (8) for this comparison. Two of the remaining variables in Eq. (5), r_p and f, can be combined into a single parameter, the effective grain diameter d_{eff} $[d_{\text{eff}} = 2(1 - f)r_p/3f]$.[21] Now the best colorimetric match occurs for $d_{\text{eff}} = 2298$ mm, which for $r_p = 0.5$ mm corresponds to $f \simeq 0.00015$. The most obvious difference between the Bohren and SDE models is that the latter predicts a smaller hemispheric albedo than the former. However, we can make this albedo difference negligible by changing our albedo error criterion and requiring that the SDE albedos err on the high side of the reconstructed albedo. (This would increase the chromaticity errors slight-

ly.) In other words, the sign of the albedo errors in this comparison of the Bohren and SDE models has no special significance.

CONCLUSIONS

Obviously the reconstructed and model spectra in Fig. 15 are not congruent. This implies that the ice in Plates I and II has inclusions that are not strictly gray. This would not surprise me, nor would I be bothered if the absorption spectrum of this ice, *sans* inclusions, were found to differ from that of Fig. 1. (However, it does not necessarily follow that any such inclusions or impurities must be green.) The important point of Fig. 15 is that, for the given daylight conditions, the reconstructed and model spectra are perceptually indistinguishable. Thus, what we see in Plates I and II *could* be the result of reddened sunlight illuminating blue-green ice that contains only a few essentially gray scatterers. My goal here is not to demonstrate that this must be the case but merely to show that, to account for what we see, only the simplest assumptions are required.

Answering the elusive question of why some icebergs are so vividly green may require as much psychophysics as it does geophysics. As an illustration, consider the following: some green iceberg photographs show that the ice undergoes a marked color shift toward the green when the sun is low in the sky.[45] Color constancy and memory color may reduce this perceptual shift for *in situ* observers. However, the reduction seems to consist of discounting the bergs' often pastel appearance near midday. Regrettably, short of sailing a group of subjects to the Weddell Sea for full-scale psychophysical testing, we are unlikely to settle any of these perceptual problems that are not addressed by colorimetry.

Ongoing physical and chemical analyses of green icebergs[13] will begin to give us definitive answers about these bergs' unique structure. However, even without such answers we can establish what the simplest requirements are for making vividly green ice. As I have shown above, there is nothing that rules out bubbly or dirty ice as the cause of at least some green icebergs. Although green icebergs might be tinted by specific colorants, in at least one case a demonstrably green iceberg contained few colored inclusions.[8] Thus the simplest explanation for green icebergs requires no extrinsic colorants but instead exploits ice's intrinsic optical properties and the reddening of daylight at low sun angles.

ACKNOWLEDGMENTS

This study was supported by National Science Foundation grant ATM-8607577. I gratefully acknowledge the assistance of Craig Bohren and Alistair Fraser in suggesting and perceptively criticizing this paper. Other colleagues at Penn State, including Dennis Thomson, Robert Crane, and Herschel Leibowitz, have offered valuable observations about particular aspects of the work.

Very special thanks are owed to Gerhard Dieckmann of the Alfred-Wegener-Institut, Bremerhaven, who provided me with the indispensable color photographs of the green iceberg seen in Plates I and II. Stephen Warren of the University of Washington has provided extremely helpful photographs of and invaluable observations on green icebergs. Anthony Amos of the University of Texas and Kendall Moulton, formerly with the Polar Programs Division of the National Science Foundation, generously loaned me some splendid green iceberg photographs that have greatly clarified vital details. Sam Colbeck of the Cold Regions Research and Engineering Laboratory and David Taylor of the University of Natal have performed the great service of prompting me and my colleagues to reconsider the question of why some icebergs are green.

REFERENCES AND NOTES

1. L. L. Noble, *After Icebergs with a Painter: A Summer Voyage to Labrador and around Newfoundland* (Appleton, New York, 1861), pp. 28, 57, 167–170.
2. A. Sparrman, *A Voyage Round the World with Captain James Cook in H.M.S. Resolution* (Golden Cockerel, London, 1944), p. 34.
3. H. O. Fletcher, *Antarctic Days with Mawson: A Personal Account of the British, Australian and New Zealand Antarctic Research Expedition of 1929–1931* (Angus and Robertson, London, 1984), pp. 121–122.
4. J. M. Wordie and S. Kemp, "Observations on certain Antarctic icebergs," Geogr. J. **81**, 428–434 (1933).
5. A. R. Binder, "Black and white icebergs," Mar. Obs. **42**, 15–16 (1972).
6. K. N. Moulton and R. L. Cameron, "Bottle-green iceberg near the South Shetland Islands," Antarct. J. U. S. **11**, 94–95 (1976).
7. A. F. Amos, "Green iceberg sampled in the Weddell Sea," Antarct. J. U. S. **13**, 63–64 (1978).
8. G. Dieckmann, C. Hemleben, and M. Spindler, "Biogenic and mineral inclusions in a green iceberg from the Weddell Sea, Antarctica," Polar Biol. **7**, 31–33 (1987).
9. The words "intrinsic color" are used as a shorthand to describe spectral absorption or reflection that is markedly selective. Properly speaking, of course, color is not an inherent physical property of objects.
10. E. Kol and E. A. Flint, "Algae in green ice from the Balleny Islands, Antarctica," N. Z. J. Bot. **6**, 249–261 (1968).
11. T. Hoshiai, "Diatom distribution in sea ice near McMurdo and Syowa Stations," Antarct. J. U. S. **7**, 84–85 (1972).
12. E. Takahashi, "Floristic study of ice algae in the sea ice of a lagoon, Lake Saroma, Hokkaido, Japan," Mem. Tokyo Natl. Inst. Polar Res. Ser. E **34**, 49–56 (1981), Plates I–IV.
13. Vin Morgan and his colleagues at the Australian Antarctic Division, University of Melbourne, are currently analyzing a green iceberg found near Mawson Station, Antarctica.
14. "Homogeneous ice" here means ice that contains no inclusions (e.g., air bubbles and diatoms); homogeneous or uniform distribution of inclusions is a separate issue.
15. S. G. Warren, "Optical constants of ice from the ultraviolet to the microwave," Appl. Opt. **23**, 1206–1225 (1984).
16. 1931 CIE colorimetric notation is used throughout. In particular, the dominant wavelength and purity of colors are measured with respect to the chromaticity of the original light source (the equal-energy spectrum here).
17. T. C. Grenfell and G. A. Maykut, "The optical properties of ice and snow in the Arctic Basin," J. Glaciol. **18**, 445–463 (1977).
18. T. C. Grenfell, "The effects of ice thickness on the exchange of solar radiation over the polar oceans," J. Glaciol. **22**, 305–320 (1979).
19. D. K. Perovich and T. C. Grenfell, "Laboratory studies of the optical properties of young sea ice," J. Glaciol. **27**, 331–346 (1981).
20. D. K. Perovich and T. C. Grenfell, "A theoretical model of radiative transfer in young sea ice," J. Glaciol. **28**, 341–356 (1982).
21. C. F. Bohren, "Colors of snow, frozen waterfalls, and icebergs," J. Opt. Soc. Am. **73**, 1646–1652 (1983), Plates VII–VIII.

22. C. F. Bohren, "Multiple scattering of light and some of its observable consequences," Am. J. Phys. **55**, 524–533 (1987).
23. P. C. Mullen and S. G. Warren, "Theory of the optical properties of lake ice," J. Geophys. Res. **93** (7), 8403–8414 (1988).
24. The factor of 2 arises in Eq. (1) because, in the large-particle limit, scatterers' extinction cross sections are twice their geometric cross sections.
25. W. S. B. Paterson, *The Physics of Glaciers*, 2nd ed. (Pergamon, Oxford, 1981), p. 6.
26. W. J. Wiscombe and S. G. Warren, "A model for the spectral albedo of snow. I: pure snow," J. Atmos. Sci. **37**, 2712–2733 (1980).
27. J. H. Joseph, W. J. Wiscombe, and J. A. Weinman, "The delta–Eddington approximation for radiative flux transfer," J. Atmos. Sci. **33**, 2452–2459 (1976).
28. "Hemispheric albedo" describes the ratio of hemispheric exitance to irradiance at any location on an ice surface. "Biconical albedo" is more general and indicates the ratio of outbound to inbound radiances that have been integrated over two specific solid angles. Unless noted otherwise, here "albedo" indicates a quantity integrated across the visible spectrum. For analogous definitions in reflectometry, see D. E. Spencer and E. A. Gaston, "Current definitions of reflectance," J. Opt. Soc. Am. **65**, 1129–1132 (1975). These distinctions are not immaterial, since instruments that preserve information about radiances, such as television cameras and our eyes, yield estimates of biconical albedo. The ice albedo models that we use are couched in terms of hemispheric albedo.
29. Note that biconical albedos and spectra are measured at observing angles where the sun's specular reflection is not visible. As such, then, R_1 will not be included in our measurements. However, since both our observations and modeling of ice albedo avoid placing the direct solar beam at grazing incidence, the external specular contribution to a_{SDE} will be small anyway.
30. R. L. Lee, Jr., "Green icebergs: a problem in geophysics and atmospheric optics," Ph.D. dissertation (Pennsylvania State University, University Park, Pa., 1989), pp. 95–99.
31. T. C. Grenfell and D. K. Perovich, "Spectral albedos of sea ice and incident solar irradiance in the southern Beaufort Sea," J. Geophys. Res. **89** (C3), 3573–3580 (1984).
32. See L. T. Maloney and B. A. Wandell, "Color constancy: a method for recovering surface spectral reflectance," J. Opt. Soc. Am. A **3**, 29–33 (1986) for a recent bibliography on measurements of daylight spectra.
33. H. R. Condit and F. Grum, "Spectral energy distribution of daylight," J. Opt. Soc. Am. **54**, 937–944 (1964).
34. S. T. Henderson, *Daylight and Its Spectrum*, 2nd ed. (Wiley, New York, 1977), pp. 83–125.
35. M. R. Nagel, H. Quenzel, W. Kweta, and R. Wendling, *Daylight Illumination: Color-Contrast Tables for Full-Form Objects* (Academic, New York, 1978), pp. 3–24.
36. M. Iqbal, *An Introduction to Solar Radiation* (Academic, New York, 1983), pp. 107–168.
37. E. J. McCartney, *Optics of the Atmosphere: Scattering by Molecules and Particles* (Wiley, New York, 1976), pp. 132–156.
38. G. E. Shaw, "Sun photometry," Bull. Am. Meteorol. Soc. **64**, 4–10 (1983).
39. R. L. Lee, Jr., Ref. 30, pp. 130–138, 168–179.
40. L. M. Hurvich, *Color Vision* (Sinauer, Sunderland, Mass., 1981), p. 209.
41. B. K. P. Horn, "Exact reproduction of colored images," Comput. Vision Graphics Image Process. **26**, 135–167 (1984).
42. R. L. Lee, Jr., "Colorimetric calibration of a video digitizing system: algorithm and applications," Color Res. Appl. **13**, 180–186 (1988).
43. C. F. Bohren and A. B. Fraser, "Colors of the sky," Phys. Teach. **23**, 267–272 (1985).
44. C. S. McCamy, H. Marcus, and J. G. Davidson, "A color-rendition chart," J. Appl. Photogr. Eng. **2**, 95–99 (1976).
45. G. Dieckmann (Alfred-Wegener-Institut für Polar- und Meeresforschung, Postfach 120161, Columbusstrasse, D-2850 Bremerhaven, Federal Republic of Germany) and S. G. Warren (Geophysics Program, AK-50, University of Washington, Seattle, Washington, 98195), personal communications.